IRAQI BULLETIN OF GEOLOGY AND MINING (IBGM)\
IRAQ GEOLOGICAL SURVEY (GEOSURV-IRAQ)

*IBGM (**2025**, Vol 21; Issue 2)* *233-250*

SEDIMENTS IN THE SOUTHERN PART OF AL-HUWAIZAH MARSH, IRAQ: DEPOSITIONAL PROPERTIES, MINERALOGY, GEOCHEMISTRY, AND PROVENANCE

Khaleel J. Al-Sudani[1], Maher M. Mahdi*[1], Mohanad H. Al-Jaberi[1], and Badir N. Albadran[2]

1 Department of Geology, College of Science, University of Basrah
2. Almaaqal University, Basrah, Iraq
* Correspondence author: maher.mahdi@uobasrah.edu.iq

Type of the Paper (Article)
Received: 07/04/2025
Accepted: 22/07/2025
Available online: 27/12/2025

Abstract

Eighteen subsurface sediment samples were collected for analysis, ten samples from site one and eight from site two in the southern part of the Al-Huwaizah marsh. The sampling depth was eight meters at site one and six meters at site two, ten samples for the first site and eight for the second site. The sediment size distribution in the study area, comprising sand, silt, and clay, was determined through grain size analysis. The textures identified in the sediments include sandy silt, silt, silty sand, and mud, with a slight fining trend observed towards the top, particularly at the first site. This fining trend suggests a gradual reduction in the load capacity of the water supplying the study area. X-ray diffraction analysis of bulk sediments revealed that the predominant minerals are quartz and calcite, followed by feldspar, halite, dolomite, and gypsum. The clay minerals, kaolinite and a mixed layer of montmorillonite–chlorite were identified to be the most abundant, with additional presence of montmorillonite, illite, chlorite, and palygorskite. The geochemical investigation highlighted a dominance of SiO_2 and CaO, succeeded by Al_2O_3, Fe_2O_3, MgO, Na_2O, SO_3, K_2O, and TiO_2. Trace elements included Cr, Co, Nb, Sr, Y, and Zr, with strontium exhibiting the highest concentration of 274.7 ppm at site two, while rubidium was the least abundant at 14.62 ppm in the same location. The relative variability of palygorskite and kaolinite minerals at different depths indicates the influence of chemical and physical weathering processes characterized by hydration and dehydration phenomena in the study area. Additionally, the sediment origins were traced back to multiple sources of igneous rocks, including rhyodacite-dacite and andesite at site one, while site two presented andesite, andesite-basalt, and sub-alkaline basalt. The Chemical Index of Alteration and Plagioclase Index of Alteration serve as indicators of weathering and suggest a reduction in chemical weathering in this region.

Keywords: Mineralogy; Geochemistry; source rocks; Clay Minerals; Al-Huwaizah Marsh; Iraq

ISSN 1811-4539, EISSN 3005-3714
https://doi.org/10.59150/ibgm2102a12
IBGM: http://ibgm-iq.org/
Academic Scientific Journals: www.iasj.net

1. Introduction

The marshes in the Mesopotamian Zone are one of the most important geomorphological features of that basin. The Al-Huwaizah Marsh is located in the eastern part of the marshland region, spanning both the Missan and northern Basrah Governorates (Figure 1). This study area represents a vital segment of the broader marshlands, which account for roughly 4% of Iraq's total land area. The region is characterized by extensive alluvial plains with minimal topographic variation, creating a unique ecological landscape. Topographically, the general slope of the area trends from northwest to southeast (Aqrawi, 1997, 2001). In the northern region of the Huwaizah Marsh, the terrain descends gradually to depths of less than 5 meters, with a gentle southward slope. Conversely, at the southern edge near Qurna, elevation increases to approximately 2 meters. During flood events, the low-lying areas are inundated, with water depths occasionally reaching around 1 meter (Lazim et al., 2024). These seasonal floods often lead to the development of sabkhas—extensive salt flats formed by the evaporation of floodwaters during the hot, arid summer months. This cyclical process plays a vital role in shaping the marsh's unique hydrological and geomorphological characteristics, contributing to its dynamic and saline environment (Sissakian et al., 2021). This dynamic interplay of hydrology not only shapes the physical landscape but also supports a wide variety of biodiversity within the marsh ecosystem. The landscape of the study area is predominantly shaped by recent Holocene deposits, which include a variety of sediment types such as aeolian deposits, depression-fill deposits, floodplain deposits, and sheet runoff deposits. The topography is characterized by the interplay of anticlines and concave structures, with these geological formations existing alongside a network of faults (Buday T, 1980; Jassim & Goff, 2006; Sissakian et al., 2017). This duality of structural features gives rise to distinct terrain types: anticlinal folds manifest as hills and highlands characterized by a smooth, uniform slope, while concave folds, or valleys, present broad and expansive areas that contribute to a diverse sedimentary landscape (Al-Dabbas et al., 2016). Situated south of the city of Missan and north of the Shatt al-Arab, the study area is encompassed within the Mesopotamian alluvial plain. This extensive region is defined by modern sediments deposited through the dynamic processes of this sedimentary basin, which lies primarily within the eastern portion of the Arabian Plate and extends into the southwestern region of the Iranian Plate. Over the millennia, the area has undergone numerous tectonic movements, with the most significant occurring during the Pliocene epoch, approximately 2 to 5 million years ago (Jassim & Goff, 2006). This period of intense geological activity resulted in notable warping of the earth's crust, leading to the formation of mountain ranges, most prominently the Zagros and Oman mountains, as well as the development of the Arabian Gulf depression, which features smaller extensions extending toward the Mesopotamian valley (Mahdi et al., 2022) In the subsequent Pleistocene epoch, roughly 2 million years ago, substantial clastic materials were deposited within the Mesopotamian basin, further shaping its present configuration. Beyond the Quaternary deposits that dominate the studied region, a distinctive landscape feature is observed in the form of alluvial fans that have emerged as a consequence of the intermittent seasonal channels that originate from Iran and traverse the territory into Iraq. These alluvial fans, formed through the deposition of sediment-laden flows, have played a significant role in shaping the region's

geomorphology (Juyal et al., 2020). The seasonal fluctuations in the channels' behavior have resulted in the accumulation of sediment, which has, in turn, created an array of alluvial fans that are characteristic of this part of the region (Aqrawi, 2001).

While there have been several prior studies on the Al-Huwaizah Marsh, the majority tend to concentrate on the dynamics of water inflow and the subsequent rejuvenation of the marshlands. In contrast, research specifically addressing sedimentary processes has been relatively scarce. Below, we will highlight the most significant studies about the marsh (Jabbar, 2008; Amin, 2014; Al-Dabbas et al., 2016; Al -Sheikhly et al., 2021; Maaroof et al., 2023). Most of these studies have thoroughly characterized the mineralogical composition of the sediments within these marshes, identifying a diverse array of mineral types. Additionally, they have critically examined the primary source rocks responsible for generating these minerals, providing valuable insights into the geological processes that influence sediment composition and mineral distribution in the region.

This study aims to elucidate the depositional conditions and sources of sediments found in the southern region of the Al-Huwaizah Marsh, thereby enhancing our understanding of the geology in this unique environment.

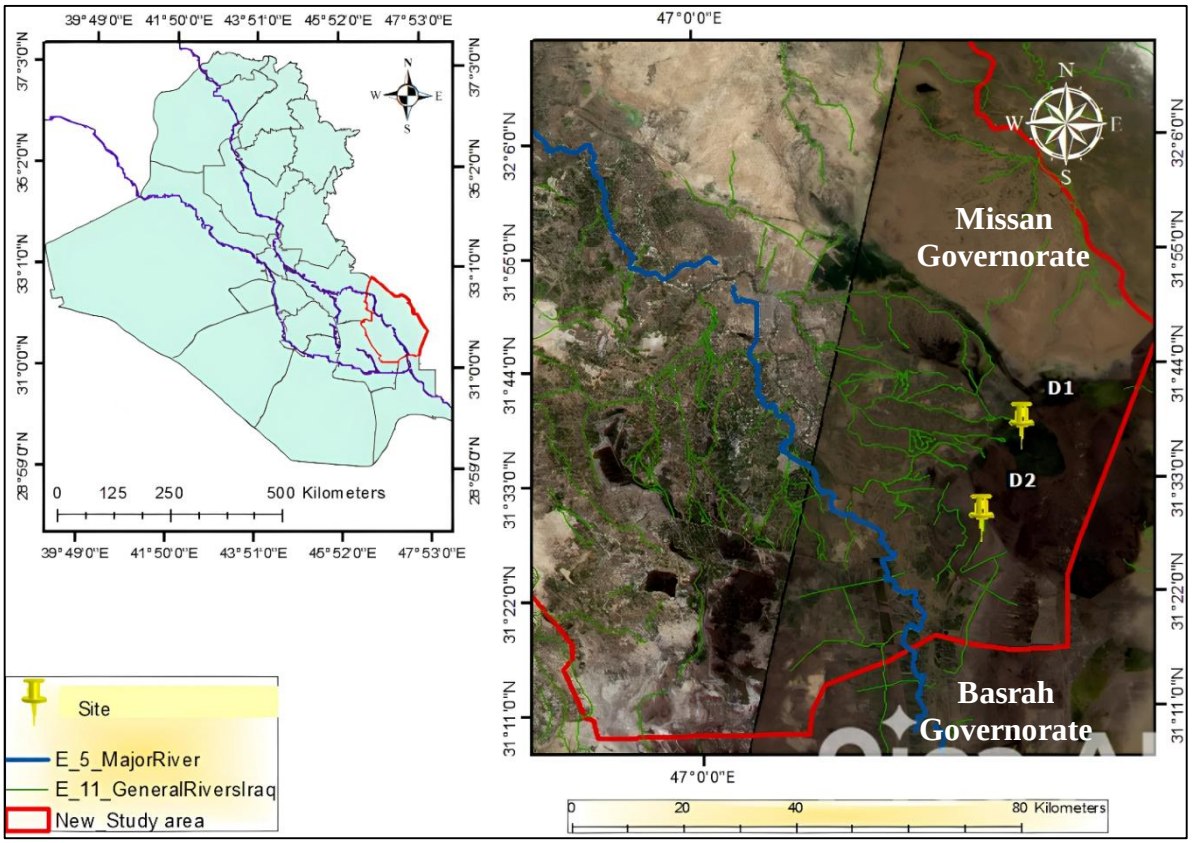

Figure 1. Location map of the studied sections, the Southern part of Al-Huwaizah Marsh.

2. Materials and methods

Grain size analysis was conducted using the wet sieving method to effectively separate the sand fraction from the silt and clay in eighteen samples. Ten samples from site one and eight samples from site two. A 230-mesh sieve was employed for this purpose. The sand retained on the sieve was collected and subsequently dried in an electric oven at a temperature of 50 °C. For the silt and clay fractions, the pipette method was utilized to determine their size distribution. Following the protocol outlined by Folk (1974). The sediment solution was placed in a graduated cylinder, to which 20 ml of Calgon (sodium hexametaphosphate) was added to enhance the separation and dispersion of the particles. The total volume was then adjusted to 1000 ml by adding distilled water, after which the cylinder was shaken thoroughly. Once it was confirmed that the clay materials were completely dispersed, samples were drawn at specific time intervals as described by Folk (1974). The results from the analysis of silt and clay were further processed by creating a cumulative curve to calculate the percentage composition of sand, silt, and clay. The sediment profiles were then generated using the Sedlog 3.0 software (Fig. 2). X-ray diffraction analysis with a Cu target, Wave: 1.54 Å at 40 kV and 30 mA at room temperature, was carried out on eight sediment powder samples to identify the bulk minerals. After removing the carbonate fraction through the application of dilute acetic acid on eight samples, for identifying the clay minerals, three oriented slides for each sample, as a normal, glycolated, and heated, were analyzed using an X-ray diffraction apparatus located in the laboratories of the Physics Department at the College of Science, University of Basrah. X-ray diffraction patterns were obtained by means of a D-5000 x-ray diffractometer, using Cukα source in wavelength, v= 1.54056Ao at 40 kV and 30 mA between 5-40o2Θ. The identification of clay minerals within the sediments of the study area was achieved by observing the distinctive basal reflections of each mineral, following the classifications established by Grim (1986), Carroll (1970), Thorez (1976), and Awadh & Al-Dabbas (2024). Furthermore, the geochemical analysis concentrated on the chemical characterization of eight samples to ascertain the proportions of the major and trace element oxides. This was accomplished using X-ray fluorescence (XRF) techniques, specifically the Ed-XRF Instrument Spectro-Xepos from Ametek Company, within the Iraqi-German Laboratory at the University of Baghdad, College of Science, Department of Geology. This comprehensive approach allowed for a robust understanding of the mineralogical and geochemical properties of the sediment.

The calculation of the chemical index of alteration (CIA) and plagioclase of alteration (PIA) is:

$$CIA = \left(\frac{Al2O3}{Al2O3 + CaO + Na2O + K2O}\right) * 100 \quad (1)$$

$$PIA = \left(\frac{Al2O3 - K2O}{(Al2O3 - K2O) + CaO + Na2O}\right) * 100 \quad (2)$$

3. Results and Discussion

The particle size distribution of the eighteen studied samples revealed a significant increase in the average percentage of silt, surpassing the average percentages of both sand and clay (Table 1). In terms of textural classification, the samples were categorized according to the framework established by Folk (1974). This classification delineates the sediment textures into sandy silt, silt, silty sand, and mud, with predominance of silty sand (Figures 2 and 3). X-ray diffraction analyses and laboratory examinations revealed the presence of several bulk minerals, including quartz, calcite, dolomite, feldspar, halite, and gypsum (Figure 4A). Among these, quartz emerged as the predominant mineral in the samples, constituting 42.46% and 42.15% of the mineral composition in sites one and two, respectively (Table 2).

Table 1. Grain size distribution and texture type of the studied samples.

Site No.	Sample	Depth(cm)	Sand %	Silt %	Clay %	Texture
Site One	Z1	0 – 20	22	68	10	Sandy silt
	Z2	40 – 70	21	69	10	Sandy silt
	Z3	130 – 170	19	72	9	Sandy silt
	Z4	230 – 300	7	85	8	Silt
	Z5	340 – 380	4	86	10	Silt
	Z6	400 – 460	53	42	5	Silty sand
	Z7	490 – 520	52	43	5	Silty sand
	Z8	550 – 580	20	66	14	Sandy silt
	Z9	615 – 645	19	68	13	Sandy silt
	Z10	670 – 800	16	82	2	Silt
	Sample	**Depth(cm)**	**Sand %**	**Silt %**	**Clay %**	Texture
Site Two	Z11	0 – 30	3	80	17	Mud
	Z12	50 – 80	4	69	27	Mud
	Z13	110 – 160	5	64	31	Mud
	Z14	180 – 240	2	73	25	Mud
	Z15	290 – 340	4	67	29	Mud
	Z16	380 – 410	56	40	4	Silty sand
	Z17	430 – 460	53	44	3	Silty sand
	Z18	470 – 600	16	81	3	Silt

Table 2: The percentage of bulk minerals in the sediments of the studied sites (%).

Site No.	Sample	Calcite	Quartz	Feldspar	Halite	Gypsum	Dolomite
Site One	Z1	43	40	5	2	2	8
	Z4	38	43	4	6	2	7
	Z6	46	44	4	3	3	-
	Z9	37	43	4	8	3	5
	Average	41	42.50	4.25	4.75	2.50	6.66
	Sample	**Calcite**	**Quartz**	**Feldspar**	**Halite**	**Gypsum**	**Dolomite**
Site Two	Z11	41	37	6	4	6	6
	Z14	43	44	8	3	2	-
	Z16	38	46	3	3	2	8
	Z18	36	42	4	8	2	8
	Average	39.50	42.25	5.25	4.50	3.00	7.33

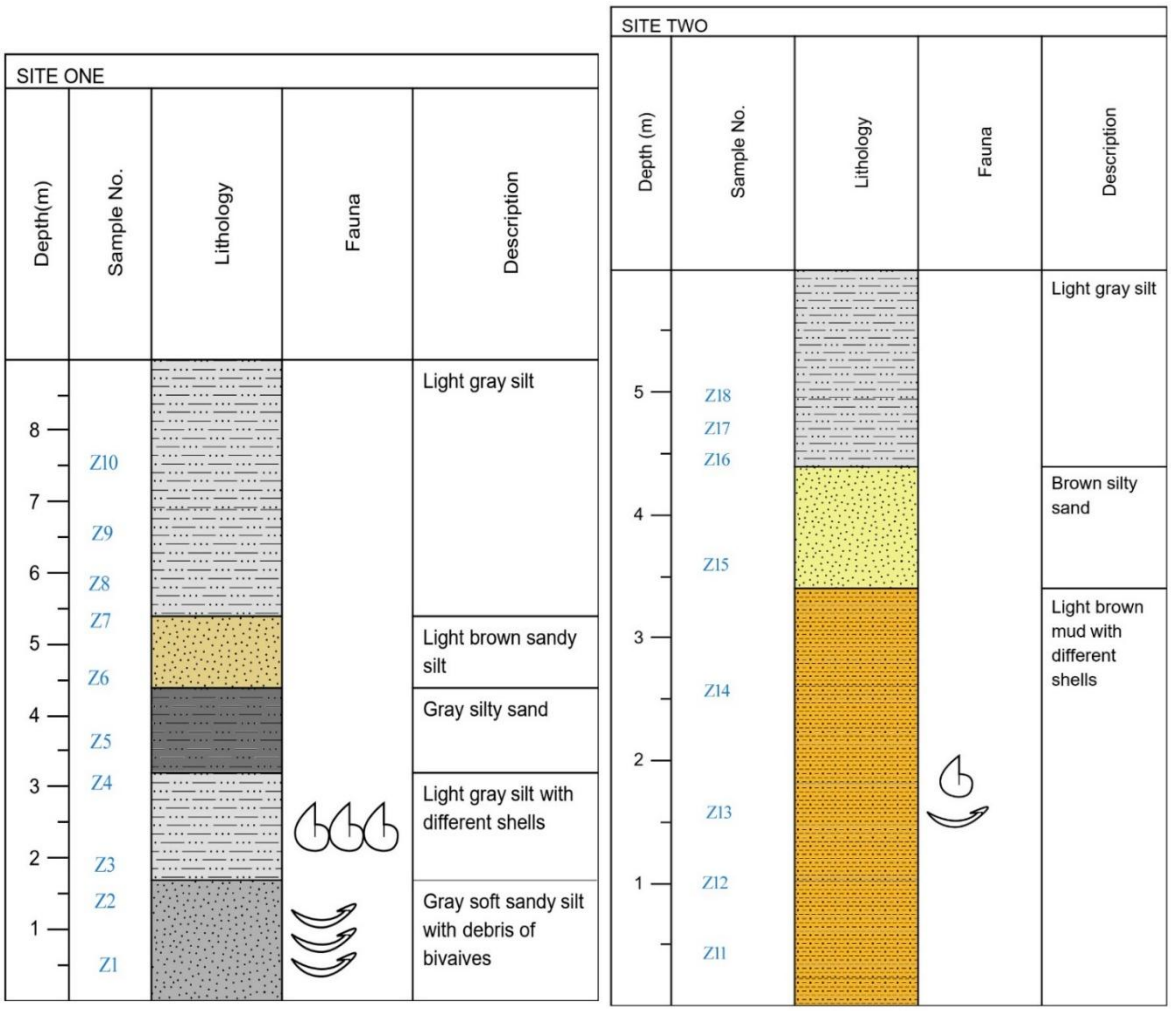

Figure 2. Lithological description of the studied boreholes.

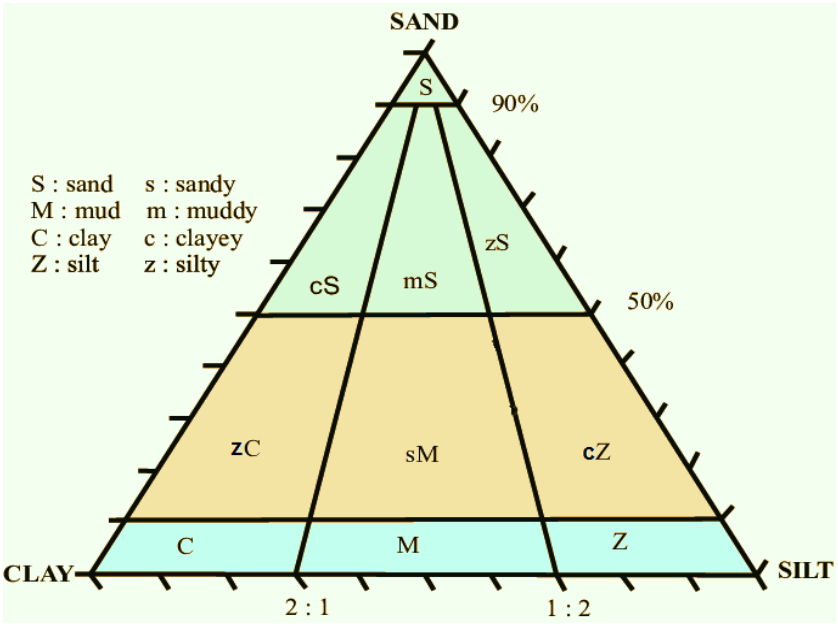

Figure 3. Texture of the studied samples according to Folk (1974).

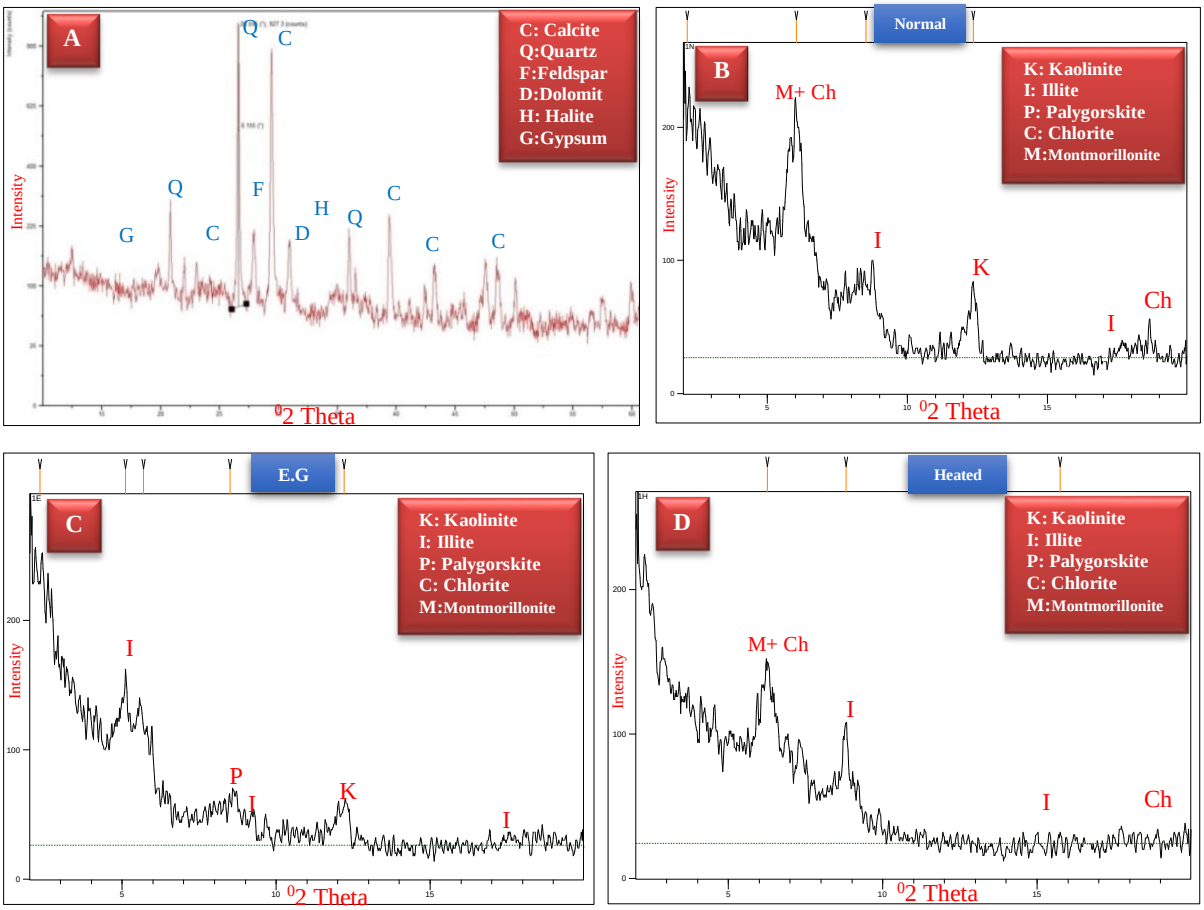

Figure 4. X-ray diffractograms of bulk minerals (A) and Orientated samples (B (normal), C (Ethylene Glycol), and D (Heated)). Sample No. Z12/Site two.

Notably, the highest percentage of quartz was recorded in sample Z16 at site two, where it ranged from 41.5% to 44.2% in site one and from 38.8% to 48.7% in site two (Table 2). The increase in quartz is manifested in the higher silica (SiO_2) content of the samples. Carbonate minerals were also identified, specifically calcite and dolomite. The X-ray diffraction results indicate that calcite was the dominant carbonate mineral, outpacing dolomite with respective mean percentages of 41.83% and 39.62% at sites one and two, respectively. The percentage range for calcite was between 34.67% and 48.48% for site one and 33.64% to 43.67% for site two. In contrast, dolomite was less prevalent, appearing in only a subset of samples with percentages of 6.98% and 7.19% for sites one and two, respectively. Feldspar was present in smaller proportions compared to quartz and calcite, with the highest concentration observed in sample Z14 at site two, averaging 4.59% and 5.09% at sites one and two, respectively. Additionally, gypsum was notable in the study area, peaking in sample Z6 at site one.

The average abundance of halite was found to be 4.68% in site one, while in site two, it was slightly higher at 5.49%. Notably, the climate has a profound impact on the variation of clay minerals. Consequently, the intensity of chemical weathering is generally lower in arid regions. Moreover, the presence of carbonate minerals, particularly calcite and dolomite, may suggest a limited extent of chemical weathering accompanied by a dry climate through the process of deposition, as posited by Xie et al. (2007). Furthermore, the predominance of light minerals suggests they likely originated from or within the sedimentary basin itself, arising through processes of sediment erosion and redeposition. The results of X-ray diffraction analyses of clay minerals for the identified samples reveal a clear dominance of kaolinite, as shown in Figures 4B, C, and D. Notably, the highest percentage of kaolinite is recorded in site one, specifically in sample Z6 (Table 3). This increase is manifested in the concurrent rise in alumina content for the same sample. Conversely, the lowest percentage of kaolinite is observed in site two, specifically in sample Z11, with averages of 24.42% and 23.32% for sites one and two, respectively. Montmorillonite is consistently identified in all of the analysed samples. The X-ray diffraction diagrams of the clay minerals reveal that the highest percentage of montmorillonite is found in sample Z1 in site one, with a corresponding increase in the concentration of the primary components that comprise montmorillonite. In contrast, the lowest percentage of montmorillonite is observed in sample Z6 (Table 3). The variations in clay mineral concentrations among samples and sites offer valuable information on the paleoclimate, weathering, and sedimentary dynamics of the study area. These results are consistent with other studies that have employed X-ray diffraction analyses to investigate the mineralogical composition of sedimentary rocks. The average percentage of montmorillonite in the analysed samples is found to be 16.87% and 15.99% for sites one and two, respectively. Chlorite was prominently evident in all analyzed samples, with its peak concentration observed in sample Z6 at site one, while the lowest concentration occurred in sample Z1 at the same site, averaging 9.18% and 9.66% for sites one and two, respectively. Goldshmidt (1970) noted that a high proportion of chlorite in certain clay deposits suggests it may have formed from the alteration of other clay minerals, particularly montmorillonite and vermiculite. Chlorite typically forms in various low-grade hydrothermal metamorphic environments, with recrystallization often occurring along fault lines (Xie et al., 2004). Illite, one of the most prevalent clay minerals in

nature, represents an intermediate state between kaolinite and montmorillonite (Al-Asha, 1991). Illite was clearly identifiable in all X-ray diffraction patterns, with the highest concentration found in sample Z1 at site one, while the lowest was recorded in sample Z9, also at site one. The average percentage of illite is approximately 13.49% in site one and 12.53% in site two. Palygorskite is also detected in all X-ray diffraction patterns, albeit at lower percentages compared to other clay minerals. Its highest concentration is observed in site one, specifically in sample Z1, while the lowest is found in sample Z9 at the same site. This prominence is manifested in the increased presence of magnesium oxide in those samples. These findings offer valuable insights into the mineralogical composition and the geological processes influencing the clay minerals within the study area. Standard analytical chemical methods were used to determine the major oxides and trace elements of the deposit samples, which included: SiO_2, CaO, Al_2O_3, Fe_2O_3, MgO, Na_2O, SO_3, K_2O, and TiO_2, while trace elements were represented by Cr, Co, Nb, Sr, Y, and Zr (Tables 4 and 5).

Table 3: The percentage of clay minerals.

Site No.	Sample	K %	I %	P %	Ch%	M%	M-Ch%
Site One	Z1	17	15	9	6	19	34
	Z4	33	18	6	9	20	14
	Z6	30	14	4	13	11	28
	Z9	28	12	4	12	24	20
	Average	27	14.75	5.75	10	18.50	24
	Sample	**K %**	**I %**	**P %**	**Ch%**	**M%**	**M- Ch %**
Site Two	Z11	20	13	9	9	15	34
	Z14	25	11	6	12	17	29
	Z16	30	16	6	10	20	18
	Z18	34	17	5	13	20	11
	Average	27.25	14.25	6.5	11	18	23

Table 4: The percentage of major element oxides (wt%).

Site No.	Sample	SiO_2 %	CaO %	Al_2O_3 %	Fe_2O_3 %	MgO %	Na_2O %	K_2O %	TiO_2 %	SO_3 %	L.O.I %
Site One	Z1	49.38	22.23	8.66	4.92	7.09	3.16	0.91	0.79	2.86	17.77
	Z4	45.98	23.29	11.36	5.76	4.95	4.40	1.44	0.66	2.16	18.93
	Z6	44.11	26.31	9.24	6.49	4.36	4.24	1.86	0.45	2.94	24.17
	Z9	48.42	24.19	8.86	6.36	3.43	4.49	1.84	1.06	1.35	20.68
	Average	46.97	24.00	9.53	5.88	4.95	4.07	1.51	0.74	2.32	20.39
	Sample	SiO_2%	CaO%	Al_2O_3%	Fe_2O_3	MgO%	Na_2O%	K_2O%	TiO_2%	SO_3%	L.O.I%
Site Two	Z11	39.63	30.45	9.40	4.82	5.76	3.76	1.64	0.67	3.87	22.73
	Z14	49.77	19.42	12.30	6.13	5.18	2.74	1.46	0.26	2.74	24.31
	Z16	52.16	21.21	10.82	5.11	4.27	1.69	1.88	0.67	2.19	19.72
	Z18	47.64	25.26	9.38	6.40	2.97	3.25	2.32	0.95	1.83	21.24
	Average	47.30	24.08	10.47	5.61	4.54	2.86	1.83	0.64	2.66	22

Table 5: The trace elements in the analysed samples (ppm).

Site No.	Sample	Cr	Co	Nb	Sr	Y	Zr
Site One	Z1	211	89	32	323	10	61
	Z4	85	35	12	159	21	20
	Z6	144	72	26	149	34	39
	Z9	89	39	13	161	39	25
	Average	132	59	21	198	26	36
	Sample	Cr	Co	Nb	Sr	Y	Zr
Site Two	Z11	444	118	9	406	23	52
	Z14	207	94	11	247	25	43
	Z16	258	78	22	268	35	47
	Z18	176	87	16	177	27	38
	Average	271	94	15	275	28	45

Silica oxide (mainly Quartz) constitutes the largest proportion among the other oxides, and this proportion is mainly related to its presence in clay minerals and feldspar and its presence in free form, i.e., in the form of quartz, which is consistent with the results of the mineral study using X-ray diffraction diagrams. The percentage of silica oxide varied between 39.56% and 43.16% for site one and between 37.37% and 46.16% for site two, yielding average values of 41.61% and 41.19% for sites one and two, respectively (Table 4). Silica oxide attained its peak concentration in sample Z16 at site two, while its lowest concentration was observed in sample Z11, also at site two. This decrease can be attributed to an increase in both calcium and sulfate content. Tables (6 and 7) illustrate the correlation relationships between silica and other oxides, revealing that silica oxide exhibits a negative correlation with both calcium oxide and sulfur oxide.

Table 6. Correlation coefficient of major oxides in site one.

	SiO_2 %	**CaO %**	**Al_2O_3 %**	**Fe_2O_3 %**	**MgO %**	**Na_2O %**	**K_2O %**	**TiO_2 %**	**SO_3 %**	**L.O.I %**
SiO_2%	1									
CaO%	-0.44	1								
Al_2O_3%	0.90	-0.72	1							
Fe_2O_3	0.10	-0.85	0.28	1						
MgO%	-0.49	-0.40	0.07	0.76	1					
Na_2O%	-0.09	-0.82	-0.51	-0.89	-0.81	1				
K_2O%	0.25	-0.76	0.13	0.99	-0.82	0.85	1			
TiO_2%	0.63	-0.55	0.50	0.20	-0.48	-0.01	0.09	1		
SO_3%	-0.21	-0.03	-0.07	-0.15	0.67	-0.51	-0.18	-0.81	1	
L.O.I%	-0.15	-0.76	0.10	0.90	-0.51	0.61	0.90	-0.45	0.27	1

Table 7. Correlation coefficient of major oxides in site two.

	SiO_2 %	**CaO %**	**Al_2O_3 %**	**Fe_2O_3**	**MgO %**	**Na_2O %**	**K_2O %**	**TiO_2 %**	**SO_3 %**	**L.O.I %**
SiO_2%	1									
CaO%	-0.67	1								
Al_2O_3 %	0.14	-0.47	1							
Fe_2O_3	0.15	-0.56	0.04	1						
MgO%	0.87	-0.62	0.39	0.55	1					
Na_2O%	0.83	0.81	-0.42	0.01	0.52	1				
K_2O%	0.55	0.19	0.88	0.11	-0.62	-0.05	1			
TiO_2%	0.26	-0.51	0.92	0.31	-0.32	-0.22	0.94	1		
SO_3%	-0.93	-0.73	-0.23	-0.48	0.98	0.68	-0.53	-0.21	1	
L.O.I%	-0.74	0.03	0.42	0.47	0.48	0.51	-0.79	-0.70	0.52	1

This suggests that the increase in carbonate minerals occurs at the expense of clay content. Additionally, silica oxide shows a negative correlation with loss on ignition and a strong negative correlation with potassium oxide, while exhibiting a robust positive correlation with aluminum and iron oxides, which are key components of clay minerals (Al-Saad, 2006). These correlations provide significant insights into the mineralogical interactions within the study area, highlighting the intricate balance between silica and other mineral constituents. Understanding these relationships enhances our comprehension of the geochemical processes influencing sediment composition and the overall mineralogical framework in the region.

The percentage of aluminum oxide varied from 7.52% to 9.69% for site one and from 7.63% to 10.51% for site two, with average values of 8.41% for site one and 9.12% for site two. The highest concentration of aluminum oxide was recorded in sample Z14 at site two, while the lowest was found in sample Z1 at site one. This trend aligns with the corresponding increases and decreases in alumina content within these two samples, highlighting their significance as primary components of clay mineral content. Aluminum oxide exhibits a strong positive correlation with potassium oxide, suggesting the presence of the clay mineral illite. It also shows a positive correlation with magnesium oxide, indicating the presence of the clay mineral palygorskite. Conversely, it demonstrates a negative correlation with both calcium oxide and sodium oxide. The concentration of titanium oxide in the sediments of the study area varied between 0.33% and 0.95% for site one, and 0.21% to 0.77% for site two, yielding average values of 0.61% for site one and 0.55% for site two. This distribution can be attributed to the substitution of titanium ions for aluminum in the crystal structure of clay minerals, a phenomenon facilitated by the similarity in their ionic radii. Additionally, titanium can replace iron and magnesium within the octahedral layer of the palygorskite (Velde, 1992).

The ratio of Al_2O_3 to TiO_2 was employed to assess climatic variations in the sediment of the study area (Kiipli et al., 2012). According to (Akul'shina, 1976), ratio values of less than 20 are indicative of humid conditions, values between 20 and 30 suggest semi-humid conditions, and values exceeding 30 indicate semi-arid climates. In this context, the samples from the study area demonstrate deposition under semi-arid conditions, as evidenced by ratio values of 32.84 and 35.26 for sites one and two, respectively (Figure 5). This observation underscores the limited chemical weathering present in the area and highlights the dominance of arid conditions.

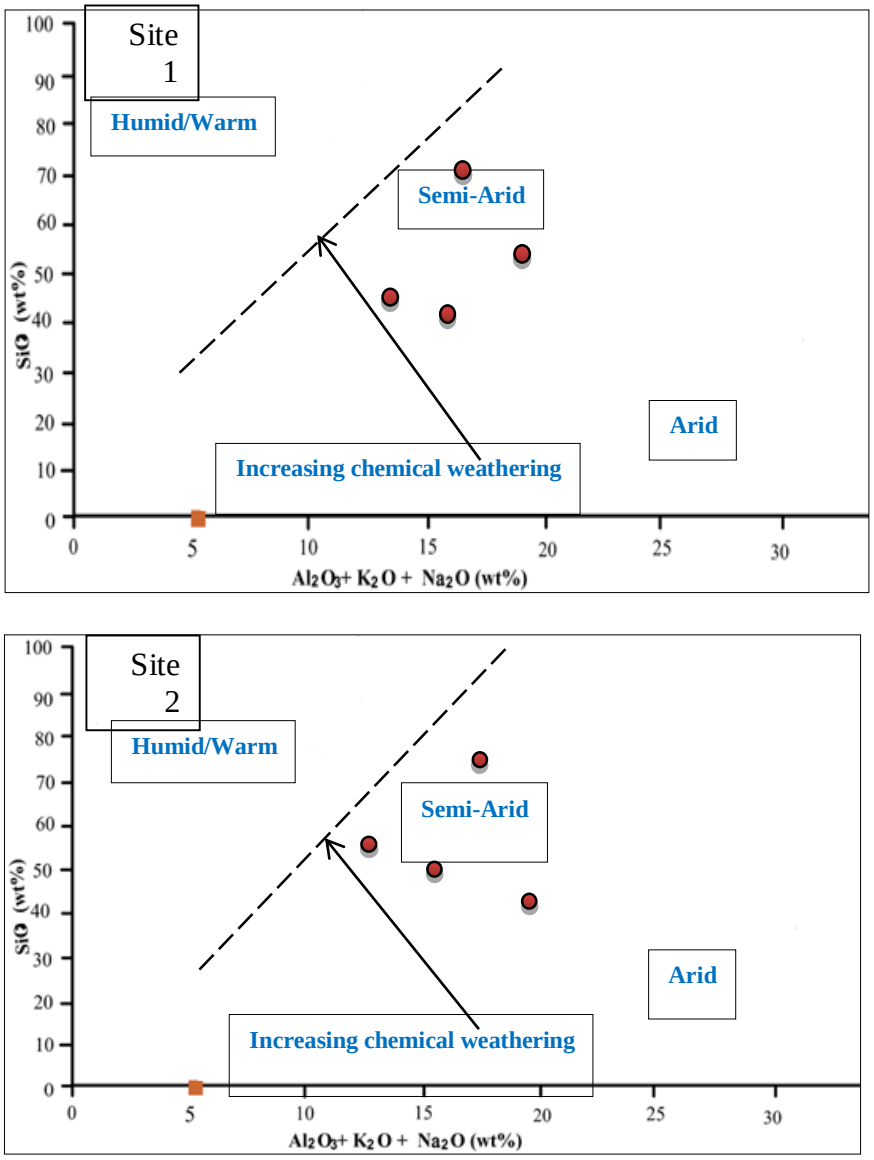

Figure 5. The ancient climate of the study area, according to Suttner & Dutta (1986).

The concentration of potassium oxide in the sediments of the study areas exhibited a wide range, varying from 0.78% to 1.76% in site one and from 1.23% to 1.89% in site two, with average values of 1.33% and 1.58% for sites one and two, respectively. The highest concentration of potassium oxide was recorded in sample Z18 at site two, while the lowest concentration was observed in sample Z1 at site one. This variation in potassium oxide levels is directly related to

the presence of the minerals illite and feldspar, which harbor potassium ions. Furthermore, potassium oxide can enter clay minerals as an exchange ion or be adsorbed onto their surfaces, including the montmorillonite mineral (Goldshmidt, 1970). The correlation relationships between potassium oxide and major oxides reinforce this interpretation. A strong positive correlation is observed between potassium oxide and silica, alumina, and iron oxides, which are the primary constituents of clay minerals, underscoring the close association between potassium oxide and clay mineral formation. In contrast, the concentration of sodium oxide ranged between 2.68% and 4.01% in site one, and between 1.47% and 3.55% in site two, with average values of 3.57% and 2.51% for sites one and two, respectively. The study area has an ancient history of arid to semi-arid climates, as depicted in Figure 5. The primary source of sodium in sediments is attributed to evaporate minerals, primarily sodium chloride and sodium sulfate, as well as to a lesser extent from clay minerals and feldspar minerals (Weaver & Pollard, 1975; Welton, 2003).

The concentration of calcium oxide in the sediments of the study area ranges from 18.86% to 24.64% for site one and from 16.59% to 28.64% for site two, with average values of 21.25% and 21.13% for sites one and two, respectively. This finding is corroborated by the significant presence of calcite observed in the X-ray diffraction patterns, alongside a minor proportion of sulfur oxide, suggesting that calcium oxide primarily exists in the form of carbonates, as further confirmed by the mineralogical X-ray diagrams. Analysis of the correlation relationships among the oxides (Table 4) reveals a strong positive correlation between calcium oxide and sulfates, which are both fundamental components of gypsum. Conversely, calcium oxide demonstrates a strong negative correlation with silica, iron, and aluminum—the primary constituents of clay minerals. Notably, the highest percentage of calcium oxide was recorded in sample Z11, which aligns with the sulfate concentration found in the same sample. In terms of iron oxide, its concentration ranged from 3.64% to 6.13% in site one and from 4.52% to 5.23% in site two, yielding average values of 5.07% and 4.87% for sites one and two, respectively. This ratio reflects the natural occurrence of iron oxide, which is integrated within the components of chlorite minerals and is also found within the crystalline structures of certain clay minerals, as well as in a free form, adsorbed onto the surfaces of clay minerals (Weaver & Pollard, 1975).

This is further substantiated by the observed positive correlations with aluminum oxide, magnesium, potassium, and titanium, alongside a strong negative correlation with calcium, sodium, and sulfate oxides. This trend indicates a decrease in the proportion of clay minerals concurrent with an increase in carbonate and sulfate minerals . The concentration of magnesium oxide varied between 3.03% and 6.02% for site one and between 2.42% and 5.25% for site two, yielding average values of 4.44% for site one and 3.96% for site two. The highest percentage of magnesium oxide was found in sample Z1, which corresponds with the mineralogical study of dolomite, where the highest concentration was similarly observed in Z1. This finding is also reflected in the X-ray diffraction diagrams of clay minerals, which show elevated percentages of both montmorillonite and illite in the same sample.

The presence of magnesium oxide in this context is thus attributed to its occurrence within dolomite and clay minerals, including palygorskite. Table 4 illustrates that magnesium oxide is strongly associated with iron, aluminum, and potassium oxides, resulting from its integration within the structural framework of clay minerals (Al-Samaani, 2009).

The data reveal a strong negative relationship between magnesium oxide and calcium oxide, highlighting the dynamic interplay between carbonate minerals; specifically, an increase in dolomite occurs at the expense of calcite. Moreover, the adsorption of elements onto these minerals tends to rise with an increase in the proportion of clay minerals (Alsaady, 2008; Mahdi & Soltan, 2021). Utilizing the Nb/Y versus Zr/TiO_2 relationship proposed by (Winchester & Floyd, 1977)The study area indicates the presence of multiple sources of diverse igneous rocks (Figure 6). As shown in Table 4, titanium oxide exhibits a robust positive correlation with silica, alumina, iron, and potassium, while displaying a negative correlation with sodium and calcium. The concentration of sulfur oxide fluctuated between 1.21% and 2.78% at site one and between 1.61% and 3.18% at site two, yielding average values of 2.09% for site one and 2.25% for site two. Notably, the highest concentration was recorded in sample Z11 at site two, whereas the lowest was found in sample Z9 at site one. Furthermore, sulfur oxide demonstrates a strong negative correlation with silica, aluminum, iron, and potassium. According to the protocol established by Nesbitt and Young (1982), the Chemical Index of Alteration (CIA) can be quantified using Equation (1) as detailed in Table 8. This metric serves as a reliable indicator of the intensity of chemical weathering, with the results illustrated in Figure 7. A comprehensive examination of the CIA values for both site one and site two, as outlined in Table 8, reveals that the source rocks in these areas have undergone a relatively low degree of weathering, consistent with the findings of Taylor & McLennan (1995).To further elucidate the weathering patterns, the Plagioclase Index of Alteration (PIA) was calculated using the formula (2), as proposed by Fedo et al. (1995). The PIA values provide valuable insights into the trends of weathering, with decreasing values indicative of a diminished degree of weathering. Notably, the calculated PIA values for both site one and site two exhibit a decline, suggesting a reduction in the intensity of weathering. This observation is congruent with the CIA results, collectively implying that the source rocks in these areas have experienced minimal chemical alteration. The integration of CIA and PIA indices offers a nuanced understanding of the weathering processes, enabling a more accurate characterization of the geochemical signature of the study area.

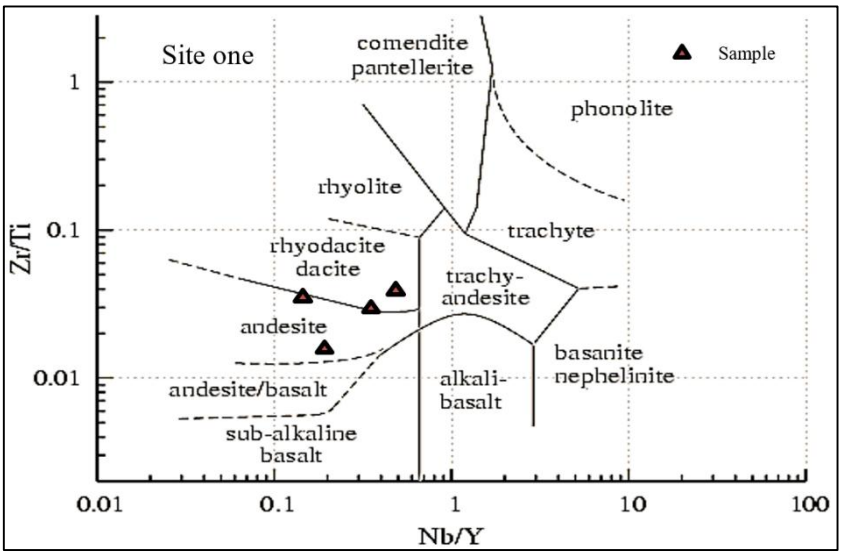

Figure 6. The distinctive source rock pertinent to the study area is represented by the red triangle after (Winchester & Floyd, 1977).

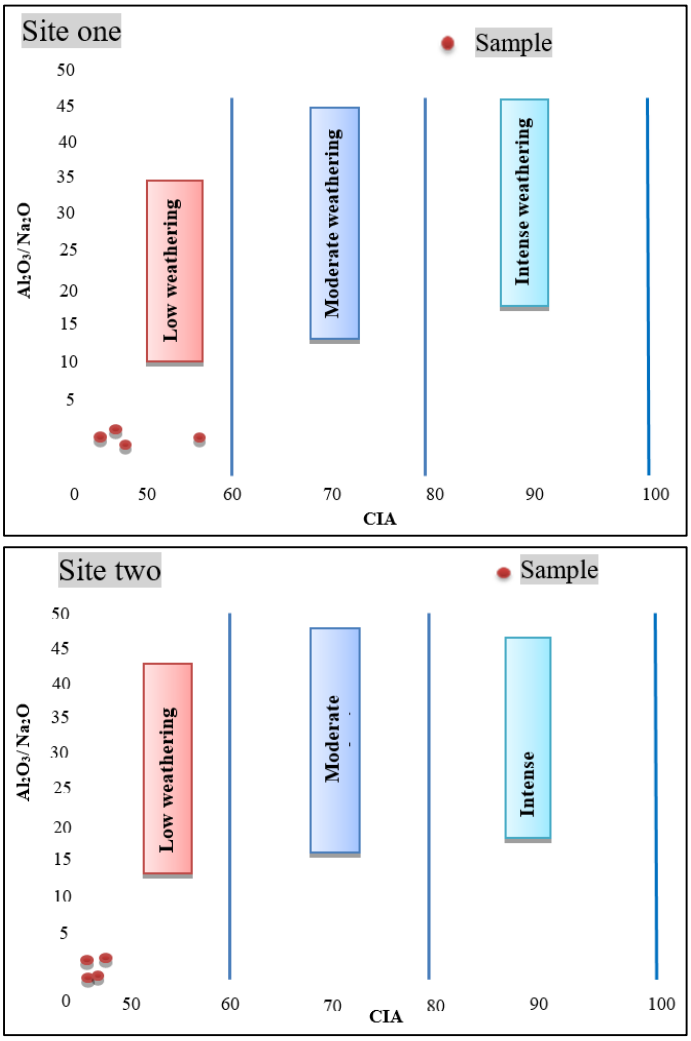

Figure 7. CIA *vs.* Al_2O_3/Na_2O for study area sites samples (acclimatized from Selvaraj & Chen, 2006).

4. Conclusions

The variability in sediment grain size at different depths within the study area underscores the influence of multiple sediment supply sources, including both riverine and aeolian processes (samples Z1 to Z18). Grain size analysis reveals a diverse range of sedimentary textures, including sandy silt, silt, silty sand, and mud. Notably, there is a slight coarsening trend towards the surface, which suggests a gradual reduction in the sediment load capacity of the water that nourishes the region.

Furthermore, the relative changes in the mineral content of palygorskite and kaolinite at varying depths provide insights into the area's responses to chemical and physical weathering, particularly through the processes of hydration and dehydration. The presence of clay minerals, such as mixed-layer clays, indicates that the ancient climate of the study area was semi-arid in nature.

In terms of sediment provenance, the analysis highlights the existence of several sources of varied igneous rocks. Specifically, site one is characterized by the presence of rhyodacite, dacite, and andesite, while site two is primarily represented by andesite, andesite-basalt, and sub-alkaline basalt. When assessed through the lenses of the Chemical Index of Alteration (CIA) and the Plagioclase Index of Alteration (PIA), both indices point to a reduction in chemical weathering over time. Collectively, these findings enrich our understanding of the sedimentological and geological dynamics at play in the study area.

References

Akul'shina. (1976). *Methods for Determining Weathering Conditions, Sedimentation and Post-sedimentary Transformations According to Clay Minerals, in Glinistye Mineraly Kak Pokazateli Litogeneza (Clay Minerals as Indicators of Rock Forming Conditions). Editor E. P. Akul'shina* (E. P., Ed.).

Al-Asha. (1991). *Principles of Soil Mechanics* (M.O., Ed.). Dar Al-Kutub for Printing and Publishing, University of Mosul.

Al-Dabbas, M. A., Al-Obaidy, A. H. M., & Abed, T. K. (2016). HYDROCHEMICAL ASSESSMENT OF THE FEED WATER IN THE WESTERN PART OF HUWAIZA MARSH, MAISSAN GOVERNORATE, SOUTH OF IRAQ. *Iraqi Geological Journal*, *39–49*(2), 46–60. https://doi.org/10.46717/igj.39-49.2.4ms-2016-12-27

Al-Saad. (2006). *Evaluation and improvement of the properties of some recent deposits in selected areas north of Basrah city for the manufacture of building bricks*.

Alsaady Y. (2008). *Environmental and mineral geochemistry of Al-Jakah Marsh, south of Al-Mashrah River, within Maysan Governorate*.

Al-Samaani J. (n.d.). *Mineralogy and geochemistry of the sandstone rocks of the Mukdadiyah Formation in selected areas, north-east of Maysan*. University of Basrah.

Amin, G. F. , Y. A. M. , A.-B. H. A. , & M. A. S. (2014). Gravity and Magnetic surveys to Delineate subsurface structure in Hor Al-Huwazah Area, South Iraq. *Iraqi Bulletin Geo. Min*, *10*(2), 59–85.

Aqrawi A. (1997). The nature and preservation of organic matter in Holocene lacustrine/deltaic sediments of lower Mesopotamia, SE Iraq. *Journal of Petroleum Geology*, *20*(1), 69–90.

Aqrawi A. (2001). Stratigraphic signatures of climatic change during the Holocene evolution of the Tigris–Euphrates delta, lower Mesopotamia. *Global and Planetary Change*, *28*(1–4), 267–283.

Awadh, S. M., & Al-Dabbas, M. (2024). *Physiography and Atmospheric Hazards. In The Geography of Iraq*. Springer Nature Switzerland.

Buday T. (1980). *The regional geology of Iraq: stratigraphy and paleography. State organization for minerals*. Al-Kutb Publishing House, Mosul.

Carroll D. (1970). Clay minerals: A guide to their X-ray Identification. *Geo. Soc. Of Amer, Special Paper*, *126*(80).

Fedo, C. M., H., Wayne Nesbitt, & Young, G. M. (1995). Unraveling the effects of potassium metasomatism in sedimentary rocks and paleosoils, with implications for paleoweathering conditions and provenance. *Geology*, *23*(10), 921–924.

Folk. R. L. (1974). *Petrology of Sedimentary Rocks* (Vol. 128). Hemphill Pub. Co., Texas, USA.

Goldshmidt, V. M. (1970). *Geochemistry*. Oxford University Press, London.

Grim, R. E. (1986). *Clay mineralogy* (2nd ed.). McGraw-Hill, New York.

Jabbar, M. F. (2008). Application of change detection techniques in Marsh Area, South Iraq. *Iraqi Bulletin of Geology and Mining*, *4*(1), 105–115.

Jassim, S. Z., & Goff, J. C. (2006). *Geology of Iraq* (1st ed.). Dolin, Praque, and Moravian Museum, Brno. Czech Republic.

Juyal, N., Singhvi, A. K., & Glennie, K. W. (2020). Chronology and paleoenvironmental significance of Quaternary desert sediment in southeastern Arabia. In Quaternary deserts and climatic change. *CRC*, 315–325.

Kiipli, E., Kiipli, T., Kallaste, T., & Siir, S. (2012). Al2O3/TiO2 ratio of the clay fraction of Late Ordovician–Silurian carbonate rocks as an indicator of paleoclimate of the Fennoscandian Shield. *Palaeogeography, Palaeoclimatology, Palaeoecology*, *365–366*, 312–320. https://doi.org/10.1016/j.palaeo.2012.10.001

Lazim, A. A., Ismail, M. J., & Mahdi, M. M. (2024). High resolution sequence stratigraphy of the Mishrif Formation (Cenomanian-Early Turonian) at Zubair Oilfield (al-rafdhiah dome), southern Iraq. *Petroleum Research*, *9*(1), 61–71. https://doi.org/10.1016/j.ptlrs.2023.08.002

Maaroof, B. F., Kareem, H. H., H. Al-Abdan, R., & Obaid, H. S. (2023). Geographical Assessment Of The Natural Environment At Al-Huwaizah Marsh, Eastern Of Misan Governorate, Iraq." *مجلة ميسان للدراسات الأكاديمية*, 188. https://doi.org/10.54633/2333-022-046-019

Mahdi, M. M., & Soltan, B. H. (2021). Determination of the Origin of Mukdadiya Formation's Gravels in Al-Teeb Region, East of Maysan Governorate, Southern Iraq, Based on Sedimentological and Paleontological Evidence. *Iraqi Journal of Science*, 2970–2982. https://doi.org/10.24996/ijs.2021.62.9.13

Maher M. Mahdi, Ismail, M. J., & Mohammad, O. A. M. (2022). The Integration of Wireline Logs and Sedimentological Data to Predict Sequence Stratigraphic Framework in Carbonate Rocks: An Example from Rumaila Formation (Cenomanian), West Qurna Oil Field, Southern Iraq. *Stratigraphy and Geological Correlation*, *30*(5), 360–377. https://doi.org/10.1134/S0869593822050045

S. Al – Al-Sheikhly, S., A. Al – Jumaily, W., S. Al - Ka'abi, F., Kh. Al – Al-Shehmany, Z., & A. Owen, M. (2021). Late Pleistocene - Holocene Paleoecology of Southern Mesopotamia, Iraq. *Iraqi Journal of Science*, 1856–1873. https://doi.org/10.24996/ijs.2017.58.4A.10

Selvaraj, K., & Chen, C. A. (2006). Moderate Chemical Weathering of Subtropical Taiwan: Constraints from Solid-Phase Geochemistry of Sediments and Sedimentary Rocks. *The Journal of Geology*, *114*(1), 101–116. https://doi.org/10.1086/498102

Sissakian, V., Abdul Ahad, A., Al-Ansari, N., & Knutsson, S. (2017). Geomorphology, geology, and tectonics of Jabal Sanam, southern Iraq. *Earth Sciences and Geotechnical Engineering*, *7*(3), 97–113.

Sissakian, V. K., Al-Ansari, N., & Adamo, N. (2021). Geomorphology, stratigraphy, and tectonics of the Mesopotamian plain, Iraq: a critical review. *Geotectonics*, *55*(1), 135–160.

Suttner, L. J., & Dutta, P. K. (1986). Alluvial sandstone composition and paleoclimate, 1. Framework mineralogy. *J Sed Petrol.*, *56*(2), 329–345.

Taylor, S. R., & McLennan, S. M. (1995). The geochemical evolution of the continental crust. *Reviews of Geophysics*, *33*(2), 241–265. https://doi.org/10.1029/95RG00262

Thorez, J. (1976). *Practical identification of clay minerals*. Belgique.

Velde, B. (1992). *Introduction to Clay Minerals*. Springer Netherlands. https://doi.org/10.1007/978-94-011-2368-6

Weaver, C. E., & Pollard, L. (1975). *The Chemistry of Clay Minerals*. Elsevier-Amsterdam.

Welton, J. E. (2003). *SEM Petrology Atlas*, (Vol. 4). The American Association of Petroleum Geologists, Chevron Oil Field Research Company, Methods in Exploration Series.

Winchester, J. A., & Floyd, P. A. (1977). Geochemical discrimination of different magma series and their differentiation products using immobile elements. *Chemical Geology*, *20*, 325–343. https://doi.org/10.1016/0009-2541(77)90057-2

Xie, M., Wang, W., De Jonge, J., & Kolditz, O. (2007). Numerical Modelling of Swelling Pressure in Unsaturated Expansive Elasto-Plastic Porous Media. *Transport in Porous Media*, *66*(3), 311–339. https://doi.org/10.1007/s11242-006-0013-0

About the author

Khaleel Jabbar Mola is a lecturer in Sedimentology at the Department of Geology, College of Science, Basrah University. He was awarded a B.Sc. in Agriculture in 2000, an M.Sc. in Sedimentology in 2015, and a Ph.D. in Sedimentology from the same university in 2022. He currently works as a lecturer and researcher in the Department of Geology, College of Science, Basrah University.

e-mail: khaleel.mola@uobasrah.edu.iq

Maher M. Mahdi earned a B.Sc. in Geology from the University of Basrah in 2000. I pursued further studies and received an M.Sc. from the same university in collaboration with Mosul University in 2003. I completed my Ph.D. in 2015 at the University of Baghdad, specializing in Stratigraphy and Paleontology. Currently, I am a professor at the University of Basrah. Scholarly contributions include 48 research papers spanning sedimentology, stratigraphy, paleontology, and petroleum geology.

e-mail (corresponding author): maher.mahdi@uobasrah.edu.iq

Mohanad H. Al-Jaberi is a professor in Sedimentology at the Department of Geology, College of Science, Basrah University. He was awarded a B.Sc. in Geology in 1998, an M.Sc. in Sedimentology in 2006, and a Ph.D. in Sedimentology from Baghdad University in 2014.
e-mail: muhanad.abood@uobasrah.edu.iq

Badir N. Albadran: Born in 1957, he received his Bachelor's degree in Geology from the University of Mosul, Iraq, in 1977, and his Ph.D. in Marine Sedimentology from the University of Nice, France, in 1986. He worked at the Marine Science Center, University of Basra, and later in the Geology Department, College of Science, University of Basra, where he became a Professor of Sedimentology in 2000. He has been the Chancellor of Almaaqal Private University in Basra since 2021.

e-mail: badir.akash@almaaqal.edu.iq